Supplement of The Cryosphere, 14, 4653–4673, 2020
https://doi.org/10.5194/tc-14-4653-2020-supplement

The Cryosphere Open Access EGU

Supplement of

The role of vadose zone physics in the ecohydrological response of a Tibetan meadow to freeze–thaw cycles

Lianyu Yu et al.

Correspondence to: Yijian Zeng (y.zeng@utwente.nl) and Zhongbo Su (z.su@utwente.nl)

Supplement

In this supplement, we first presented the constitutive equations regarding unfrozen water content, the ice effect on hydraulic conductivity, the temperature dependence of water flow, water vapor density in Section S1. Then Section S2 presented the surface fluxes simulations for the frozen/unfrozen periods. Tables were listed in Section S3.

S1 Constitutive equations

S1.1 Unfrozen water content

In both T&C and STEMMUS, the soil freezing characteristic curve (SFCC) method was employed to estimate unfrozen water content, in combination with the van Genuchten soil water retention curve (SWRC) model (Van Genuchten, 1980) and Clapeyron equation. The SWRC is expressed as

$$\theta_{tot}(h) = \begin{cases} \theta_r + \frac{\theta_s - \theta_r}{[1+|\alpha h|^n]^m}, & h < 0 \\ \theta_s, & h \geq 0 \end{cases}, \quad \text{(S1)}$$

where θ_{tot}, θ_s, and θ_r are the total water content, saturated water content and the residual water content, respectively; h (m) is the pre-freezing soil water potential; α is related to the inverse air-entry pressure; m is the empirical parameter. The parameter m is a measure of the pore-size distribution and can be expressed as m = 1-1/n, which in turn can be determined by fitting van Genuchten's analytical model (Van Genuchten, 1980).

The unfrozen water content was estimated by employing SFCC (Dall'Amico, 2010; Dall'Amico et al. 2011)

$$\theta_L(h,T) = \theta_r + \frac{\theta_s - \theta_r}{[1+|\alpha(h+h_{Frz})|^n]^m}, \quad \text{(S2)}$$

where θ_L is the liquid water content, L_f (J kg^{-1}) is the latent heat of fusion, g (m s^{-2}) is the gravity acceleration, T_0 (273.15 ^{o}C) is the absolute temperature. h, α, n, and m are the same as in S1. h_{Frz} (m) is the soil freezing potential.

$$h_{Frz} = \frac{L_f}{gT_0}(T - T_0) \cdot H(T - T_{CRIT}), \quad \text{(S3)}$$

where T (^{o}C) is the soil temperature. H is the Heaviside function, whose value is zero for negative argument and one for positive argument, T_{CRIT} (^{o}C) is the soil freezing temperature.

$$T_{CRIT} = T_0 + \frac{ghT_0}{L_f}, \quad \text{(S4)}$$

S1.2 Hydraulic conductivity

In both T&C and STEMMUS, the unsaturated hydraulic conductivity (Van Genuchten, 1980, Mualem 1976) is expressed as

$$K_{Lh} = K_s K_r = K_s S_e^l [1 - (1 - S_e^{1/m})^m]^2, \quad \text{(S5)}$$

$$S_e = \frac{\theta - \theta_r}{\theta_s - \theta_r}, \quad \text{(S6)}$$

$$m = 1 - 1/n, \quad \text{(S7)}$$

where K_{Lh}, K_s and K_r (m s^{-1}) are hydraulic conductivity, saturated hydraulic conductivity and relative hydraulic conductivity, respectively. S_e is the effective saturation. *l*, *n*, and *m* are the van Genuchten fitting parameters.

The blocking effect of ice presence is estimated by the impedance factor,

$$K_{fLh} = 10^{-EQ} K_{Lh}, \quad \text{(S8)}$$

$$Q = (\rho_i \theta_{ice} / \rho_L \theta_L), \quad \text{(S9)}$$

where K_{fLh} (m s^{-1}) is the hydraulic conductivity in frozen soils; K_{Lh} (m s^{-1}) is the hydraulic conductivity in unfrozen soils at the same negative pressure or liquid moisture content; θ_{ice} is soil ice content; *Q* is the mass ratio of ice to total water, and *E=7* is the empirical constant that accounts for the reduction in permeability due to the formation of ice (Hansson et al., 2004).

S1.3 Temperature dependence of matric potential and hydraulic conductivity

Soil matric potential and hydraulic conductivity are dependent on temperature in STEMMUS (Zeng and Su, 2013), which affects soil water surface tension and viscous flow effects. The temperature dependence of matric potential can be expressed as

$$h_{Cor\_T} = he^{-C_\psi (T - T_r)} \quad \text{(S10)}$$

where, h_{Cor_T} is the soil matric potential considering temperature effect; C_ψ is the temperature coefficient, assumed to be constant as 0.0068 $^oC^{-1}$ (Milly, 1984); T_r is the reference temperature (20 ^oC).

Hydraulic conductivity, taken into account the temperature effect, can be written as

$$K(\theta,T) = K_s K_r(\theta) K_T(T) \quad \text{(S11)}$$

where $K_r(\theta)$ is the relative hydraulic conductivity, $K_T(T)$ is the temperature coefficient of hydraulic conductivity, expressed as

$$K_T(T) = \frac{\mu_w(T_r)}{\mu_w(T)} \quad \text{(S12)}$$

where μ_w is the viscosity of water. The dynamic viscosity of water can be written as

$$\mu_w = \mu_{w0} \exp\left[\frac{\mu_1}{R(T+133.3)}\right] \quad \text{(S13)}$$

where μ_{w0} is the water viscosity at the reference temperature, μ_1=4.7428 (kJ mol^{-1}), R =8.314472 (J mol^{-1} ^{o}C^{-1}), T is the temperature in ^{o}C.

S1.4 Water vapor density

Vapor flow, driven by the gradient of water vapor density, links the water flow and heat flow in STEMMUS. The water vapor density, according to Kelvin's law, is expressed as a function of both temperature and matric potential (Philip and Vries, 1957)

$$\rho_V = \rho_{sV} H_r, \quad H_r = \exp\left(\frac{hg}{R_V T}\right), \quad \text{(S14)}$$

where ρ_{sV} is the density of saturated water vapor ($\exp\left(31.3716 - \frac{6014.79}{T} - 7.92495 \times 10^{-3} T\right) \frac{10^{-3}}{T}$); H_r is the relative humidity; R_V (461.5 J kg^{-1} K^{-1}) is the specific gas constant for vapor; g is the gravitation acceleration; T is the temperature in K.

S2 Surface Fluxes Simulations

The difference between model simulated and the eddy covariance measured 5-day moving average dynamics of surface energy fluxes was shown in Figure S1. Three models generated similar simulation patterns against the observations. The simulation of *Rn* is characterized as the overall overestimation, with isolated underestimation episodes, which occurred mainly in the frozen periods. Compared with unCPLD and unCPLD-FT model simulations, CPLD model presented a larger overestimation of *Rn*. Such overestimation tended to enlarge during the non-growing periods. There is a negligible difference of *Rn* between unCPLD and unCPLD-FT model simulations.

For H dynamics, model differences presented the seasonal variations with the general overestimation during the growing seasons while the underestimation during the non-growing seasons. During the growing season, the modeling discrepancies appeared larger in 2016 and 2018 than that in 2017. It is difficult to attribute such a difference mostly to the model inaccuracy or mostly to the data inaccuracy. On one hand, the energy balance closure problem rises as the potential source of error and reason of discrepancy. The Eddy covariance observed LE and mostly H fluxes are underestimated when constrained by the surface energy closure during the summer periods (see Table 2). On the other hand, in T&C model, the surface temperature is simplified and 'one single prognostic surface temperature' is computed, i.e. soil surface and vegetation surface temperature have the same value. The difference between the soil surface, vegetation surface and the assumed surface temperature can be a potential cause for such discrepancies in H. In addition, the uncertainties in the precipitation measurements can be an additional potential reason for the simulated differences between 2016 & 2018 and 2017.

CPLD model generated less overestimation of H, compared with unCPLD and unCPLD-FT model. As the main difference among the three models is that CPLD model taking into account the coupling water and heat physics during the unfrozen period. We attributed such difference to the water-heat coupling physics, i.e., the vapor flow effect and thermal effect on liquid flow. During the frozen periods, CPLD model usually produced a larger underestimation than unCPLD and unCPLD-FT models. Slightly better performance was identified during the late winter periods for CPLD model, probably due to the better capture of vegetation dynamics.

There are seasonal fluctuations of model performance regarding LE dynamics, with the general overestimation during the growing season while good fits during the non-growing season. The differences among the three models were minimal except some observable differences during the vegetation onset periods when the difference of vegetation dynamics occurred.

The correlation between observed and model simulated daily average surface energy fluxes for the non-frozen and frozen period was presented as Figure S2 and Figure S3. For the non-frozen period, three models can well simulate the dynamics of *Rn* except at the low radiation values. The correlation between model simulated and measured LE was weaker than *Rn*. The worst model performance was identified for H

simulations. Three models produced a similar correlation to the observed surface fluxes during the non-frozen period.

For the frozen period, the model performance degraded for the surface energy fluxes. There is a considerable underestimation of *Rn* against the measured high *Rn* values. This is probably due to the snow cover dynamics were not well captured and the uncertainties in precipitation measurements. Other than these periods, CPLD model produced overestimation of *Rn*, which results in a worse correlation than that from unCPLD and unCPLD-FT models. There is no significant difference among the three models in LE simulations. The correlation between model simulated and observed H dynamics appeared the same for the three models, while CPLD model produced the underestimation of H compared with unCPLD and unCPLD-FT simulations.

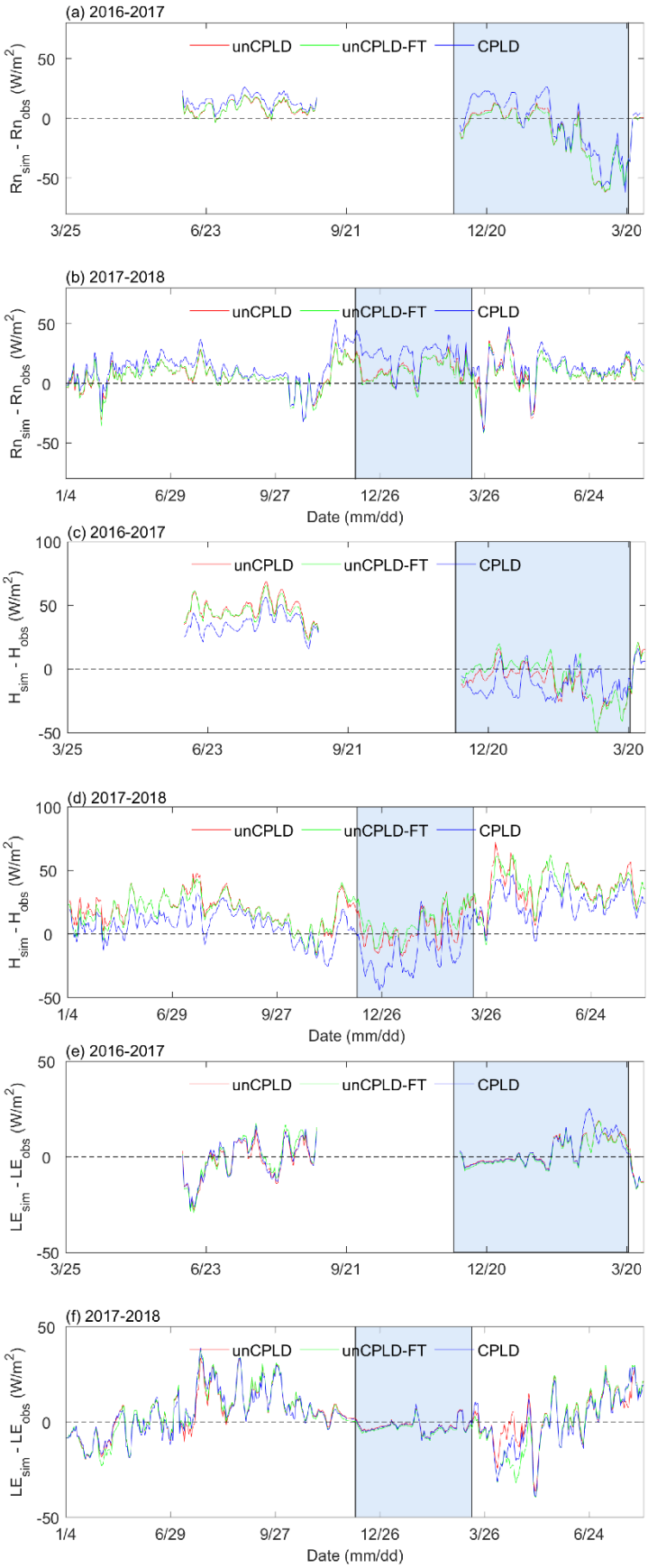
(a) 2016-2017
unCPLD
unCPLD-FT
CPLD
Rn_sim - Rn_obs (W/m^2)
50
0
-50
3/25
6/23
9/21
12/20
3/20
(b) 2017-2018
unCPLD
unCPLD-FT
CPLD
Rn_sim - Rn_obs (W/m^2)
50
0
-50
1/4
6/29
9/27
12/26
3/26
6/24
Date (mm/dd)
(c) 2016-2017
unCPLD
unCPLD-FT
CPLD
H_sim - H_obs (W/m^2)
100
50
0
-50
3/25
6/23
9/21
12/20
3/20
(d) 2017-2018
unCPLD
unCPLD-FT
CPLD
H_sim - H_obs (W/m^2)
100
50
0
-50
1/4
6/29
9/27
12/26
3/26
6/24
Date (mm/dd)
(e) 2016-2017
unCPLD
unCPLD-FT
CPLD
LE_sim - LE_obs (W/m^2)
50
0
-50
3/25
6/23
9/21
12/20
3/20
(f) 2017-2018
unCPLD
unCPLD-FT
CPLD
LE_sim - LE_obs (W/m^2)
50
0
-50
1/4
6/29
9/27
12/26
3/26
6/24
Date (mm/dd)

Figure S1. Difference between observed and simulated 5-day moving average dynamics of net radiation (Rn), latent heat flux (LE), and sensible heat flux (H) using the original (uncoupled) T&C (unCPLD), T&C with consideration of FT process (unCPLD-FT) and coupled T&C and STEMMUS (CPLD) model. The frozen period, identified from Figure 1b, was highlighted by the blue shadow.

Non-frozen period

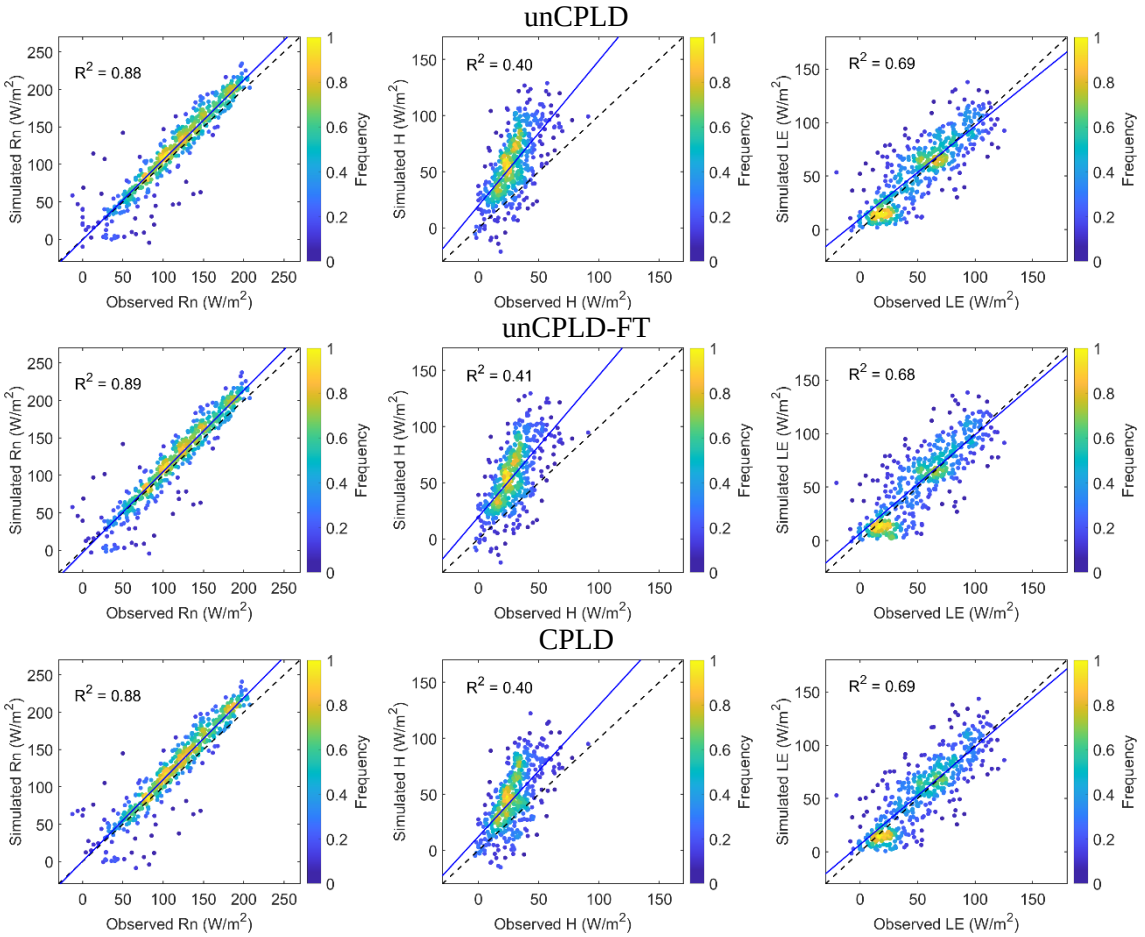

Figure S2. Scatter plots of observed and model simulated daily average surface fluxes (net radiation: Rn, latent heat: LE and sensible heat flux: H) using the original (uncoupled) T&C (unCPLD), T&C with consideration of FT process (unCPLD-FT) and coupled T&C and STEMMUS (CPLD) model during the non-frozen period, with the color indicating the occurrence frequency of surface flux values.

Frozen period

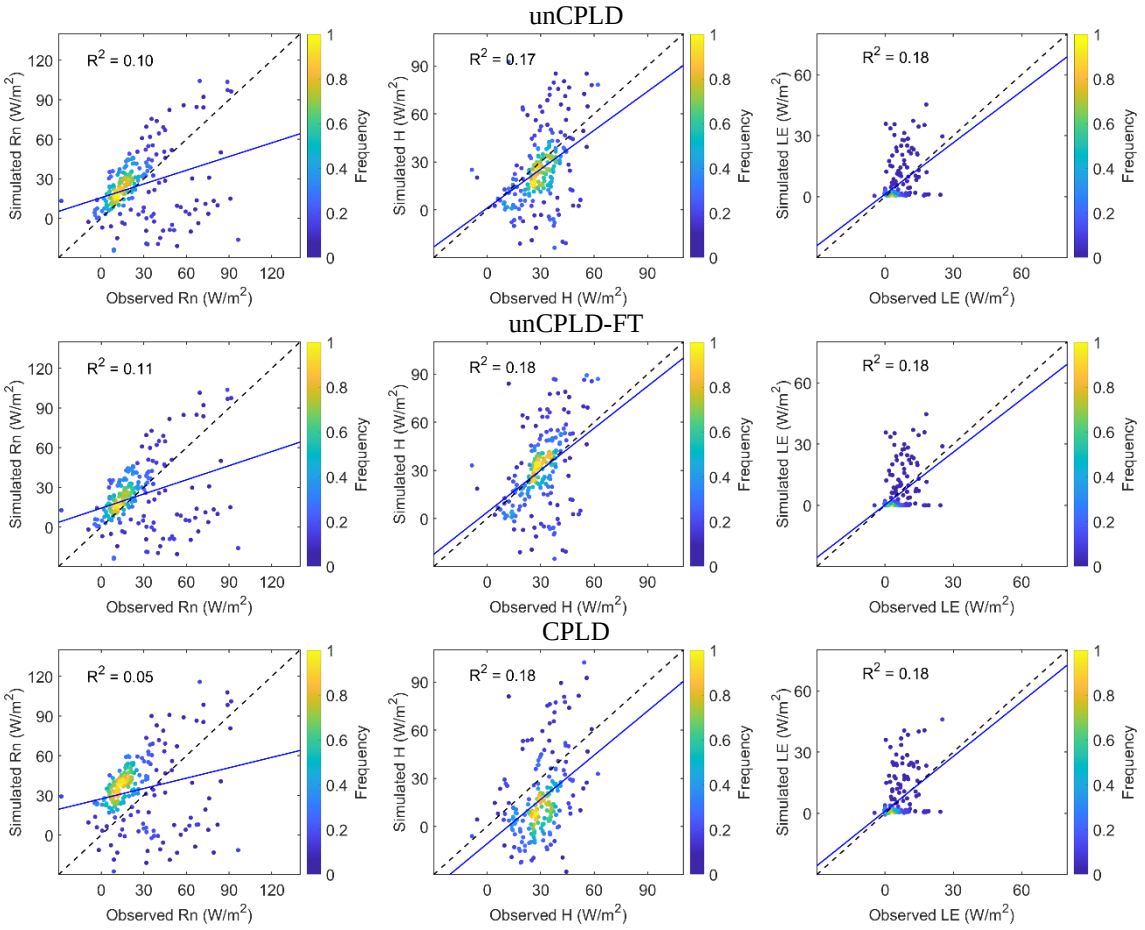

Figure S3. Scatter plots of observed and model simulated daily average surface fluxes (net radiation: Rn, latent heat: LE and sensible heat flux: H) using the original (uncoupled) T&C (unCPLD), T&C with consideration of FT process (unCPLD-FT) and coupled T&C and STEMMUS (CPLD) model during the frozen period, with the color indicating the occurrence frequency of surface flux values.

S3 Tables

Table S1. The average values of soil texture and hydraulic properties at different depths used in all simulations.

Soil depth (cm)	Clay (%)	Sand (%)	K_s (10^{-6} m s^{-1})	θ_s (cm^3 cm^{-3})	VG model θ_r (cm^3 cm^{-3})	α (m^{-1})	n
5-10	10.00	27.00	1.05	0.55	0.050	0.015	1.35
10-40	8.00	28.00	1.94	0.55	0.050	0.008	1.45
40-80	8.00	47.00	5.61	0.50	0.052	0.008	1.50

Note: VG, Van Genuchten (Van Genuchten, 1980)

120

Table S2. The main vegetation parameters for the Tibetan meadow ecosystem used in all simulations

Parameter	Symbol	Unit	Value
Root depth that contains 95% of fine root biomass	$Z_{R,95}$	m	0.3
Water use efficiency parameter, which connects the stomatal aperture and net assimilation	a_1	-	5
Specific leaf area	S_{LAI}	m^2 LAI g C^{-1}	0.0225
Maximum rubisco capacity	Vc_{max}	-	60
Temperature for leaf onset	T_{lo}	°C	0.2
Daylight threshold for senescence	L_{day_cr}	h	11.4
Cold control on leaf shedding	T_{cold}	°C	0
Water potential at 2% loss stomatal conductivity	$\psi_{S,00}$	MPa	-0.8
Water potential at 50% loss stomatal conductivity	$\psi_{S,50}$	MPa	-2.8
Critical leaf age	A_{cr}	d	180
Leaf onset water stress	β_R	-	0.99

Table S3. A summary of annual average GPP and NEE of grassland over the Tibetan Plateau, with records of mean annual temperature (MAT) and precipitation (APT)

Site	Location	Elevation (m)	Type	MAT (°C)	APT (mm)	GPP (gC m^{-2} yr^{-1})	NEE (gC m^{-2} yr^{-1})	Reference
Arou	38°3′N, 100°27′36″E	3033	grassland	0.6	464.1	818.3	-198.7	(Sun et al., 2019)
Damxung[a]	30°28′08.50″ N, 91°03′44.50″E	4286	swamp meadow	-	-	755-935	-	(Bai et al., 2011)
Damxung[a]	30°28′08.50″ N, 91°03′44.50″E	4286	swamp meadow	1.8	475.6	835.29 (755.02-901.37)	-	(Niu et al., 2016)
Damxung[a]	30°28′08.50″ N, 91°03′44.50″E	4286	swamp meadow	1.3	335	-	-161.85	(Niu et al., 2017)
Haibei[a]	38°37′N, 101°18′E	3250	shrub meadow	-1	566	634 (575-681)	-121(-193 ~ -79)	(Kato et al., 2006)
Haibei[a]	37°35′N, 101°20′E	3250	alpine wetland meadow	-1.1	510.367	629.87 (575.7-682.9)	106.1 (44-173.2)	(Zhao et al., 2010)
Lijiang	27°100′ N, 100°140′ E	3560	alpine meadow	6.1	1180	600 (522-669)	-161 (-213 ~ -114)	(Wang et al., 2017)
Zoige[a]	33°56′ N, 102°52′ E	3430	swamp meadow	-	-	589.8-672.1	-	(Tian et al., 2003)
Zoige[a]	33°56′ N, 102°52′ E	3430	swamp meadow	1.1	650	-	-79.7~-47.1	(Hao et al., 2011)
10 sites	-	3033-4730	alpine grassland	-	-	300-400	-	(He et al., 2014)

Note: [a] indicates same site with different years

Reference

Bai, J., Xu, X., Song, M., He, Y., Jiang, J., and Shi, P.: Effects of temperature and added nitrogen on carbon mineralization in alpine soils on the Tibetan Plateau, Ecology and Environmental Sciences, 855-859, 2011.

Dall'Amico, M.: Coupled water and heat transfer in permafrost modeling, University of Trento, 2010.

Hansson, K., Šimůnek, J., Mizoguchi, M., Lundin, L. C., and van Genuchten, M. T.: Water flow and heat transport in frozen soil: Numerical solution and freeze-thaw applications, Vadose Zone J, 3, 693-704, 2004.

Hao, Y. B., Cui, X. Y., Wang, Y. F., Mei, X. R., Kang, X. M., Wu, N., Luo, P., and Zhu, D.: Predominance of Precipitation and Temperature Controls on Ecosystem CO2 Exchange in Zoige Alpine Wetlands of Southwest China, Wetlands, 31, 413-422, 10.1007/s13157-011-0151-1, 2011.

He, H., Liu, M., Xiao, X., Ren, X., Zhang, L., Sun, X., Yang, Y., Li, Y., Zhao, L., Shi, P., Du, M., Ma, Y., Ma, M., Zhang, Y., and Yu, G.: Large-scale estimation and uncertainty analysis of gross primary production in Tibetan alpine grasslands, Journal of Geophysical Research: Biogeosciences, 119, 466-486, 10.1002/2013jg002449, 2014.

Kato, T., Tang, Y., Gu, S., Hirota, M., Du, M., Li, Y., and Zhao, X.: Temperature and biomass influences on interannual changes in CO2 exchange in an alpine meadow on the Qinghai-Tibetan Plateau, Global Change Biology, 12, 1285-1298, 10.1111/j.1365-2486.2006.01153.x, 2006.

Milly, P. C. D.: A Simulation Analysis of Thermal Effects on Evaporation From Soil, Water Resour Res, 20, 1087-1098, 10.1029/WR020i008p01087, 1984.

Mualem, Y.: New model for predicting the hydraulic conductivity of unsaturated porous media, Water Resour Res, 12, 513-522, 1976.

Niu, B., He, Y., Zhang, X., Fu, G., Shi, P., Du, M., Zhang, Y., and Zong, N.: Tower-Based Validation and Improvement of MODIS Gross Primary Production in an Alpine Swamp Meadow on the Tibetan Plateau, Remote Sensing, 8, 592, 2016.

Niu, B., Yongtao, H., Xianzhou, Z., Mingyuan, D., Peili, S., Wei, S., and Leiming, Z.: CO2 Exchange in an Alpine Swamp Meadow on the Central Tibetan Plateau, Wetlands, 37, 525-543, 10.1007/s13157-017-0888-2, 2017.

Philip, J. R., and Vries, D. A. D.: Moisture movement in porous materials under temperature gradients, Eos, Transactions American Geophysical Union, 38, 222-232, 10.1029/TR038i002p00222, 1957.

Sun, S., Che, T., Li, H., Wang, T., Ma, C., Liu, B., Wu, Y., and Song, Z.: Water and carbon dioxide exchange of an alpine meadow ecosystem in the northeastern Tibetan Plateau is energy-limited, Agr Forest Meteorol, 275, 283-295, https://doi.org/10.1016/j.agrformet.2019.06.003, 2019.

Tian, Y., Xiong, M., Xiong, X., and Song, G.: The organic carbon distribution and flow in wetland soil-plant system in ruoergai plateau, Acta Phytoecologica Sinica, 490-495, 2003.

Van Genuchten, M. T.: A closed-form equation for predicting the hydraulic conductivity of unsaturated soils, Soil Sci Soc Am J, 44, 892-898, 1980.

Wang, L., Liu, H., Sun, J., and Shao, Y.: Biophysical effects on the interannual variation in carbon dioxide

exchange of an alpine meadow on the Tibetan Plateau, Atmos Chem Phys, 17, 5119-5129, 10.5194/acp-17-5119-2017, 2017.

Zeng, Y. J., and Su, Z. B.: STEMMUS : Simultaneous Transfer of Engery, Mass and Momentum in Unsaturated Soil, ISBN: 978-90-6164-351-7, University of Twente, Faculty of Geo-Information and Earth Observation (ITC), Enschede, 2013.

Zhao, L., Li, J., Xu, S., Zhou, H., Li, Y., Gu, S., and Zhao, X.: Seasonal variations in carbon dioxide exchange in an alpine wetland meadow on the Qinghai-Tibetan Plateau, Biogeosciences, 7, 1207-1221, 10.5194/bg-7-1207-2010, 2010.